Proceedings of the EuroGNC 2013, 2nd CEAS Specialist Conference
on Guidance, Navigation & Control, Delft University of Technology,
Delft, The Netherlands, April 10-12, 2013

Online Estimation of Mean Orbital Elements with Control Inputs

Weichao Zhong*
Harbin Institute of Technology, Harbin 150001, China
and
Pini Gurfil†
Technion – Israel Institute of Technology, Haifa 32000, Israel

Abstract Estimating the mean orbital elements is essential for satellite orbit determination as well as guidance and autonomous orbital transfer. Whereas offline estimation of mean elements can be performed using batch processing and analytical satellite theories, online estimation requires recursive filtering. This paper proposes a unique formulation for mean orbital elements estimation, wherein the semianalytical theory is used for generating both the process and measurement equations, but the mean elements estimation is performed using an Unscented Kalman Filter. A comprehensive performance evaluation for both controlled and uncontrolled orbits shows the potential applicability of the method and its advantages compared to Brouwer-based approaches.

1 Introduction

In many cases of practical interest, satellite guidance and orbit control laws utilize mean orbital elements, rather than osculating elements, as inputs. This pertains both for open-loop and closed-loop guidance and control [1,2]. The use of mean elements – which are usually defined as a single-period-averaged osculating elements – has clear benefits, including reduced sensitivity to high-frequency content and short-periodic oscillations, which implies much lower fuel consumption. It makes more sense to have the satellite track an orbit defined by mean elements than have it respond to the fast variations of the osculating elements. This observation holds both for single- and multiple-satellite missions [3].

With the onset of autonomous satellite missions, capable of performing closed-loop autonomous orbital transfer [4], the importance of efficient on-board mean elements estimation becomes evident. Whereas in traditional satellite missions the

* Ph.D. Candidate, Research Center of Satellite Technology, Visiting Student, Distributed Space Systems Lab, Faculty of Aerospace Engineering, Technion. Email: zhongweichaohit@gmail.com

† Associate Professor, Distributed Space Systems Lab, Faculty of Aerospace Engineering. Email: pgurfil@technion.ac.il

mean elements can be estimated on the ground and uploaded to the satellites within the visibility slots, autonomous missions must be capable of producing real-time mean element estimates based on measurements obtained from the on-board sensors – typically GPS receivers.

In general, there are three main alternatives for estimating the mean orbital elements. The first is to use an analytical theory, such as the Brouwer artificial satellite theory [5], the Kozai theory [6], the drag-extended Brouwer theory [7], or newer theories, including those discussed in Refs. [8–15] to name only a few. The second alternative is to use batch processing to convert from osculating to mean elements using least-square-type approaches. Both of these alternatives could be problematic: Brouwer-type theories are sensitive to noise and modeling errors and cannot easily accommodate thrust; and batch processing is not adequate for real-time on-board implementation as it requires data accumulation for at least a complete orbital period (in addition, the actual orbital period changes, which may introduce additional errors).

The third alternative, which is the focus of the current work, is to use recursive filtering to estimate the mean elements. This approach has not received much attention in the literature, and there are only a handful of works that consider on-board mean elements estimation from osculating elements measurements [4]. This problem is not trivial, since it is difficult to write a good dynamical model for mean element propagation, formulate a mapping from mean elements back to osculating elements to get a measurement-type equation, and in addition find a filter that would be capable of properly processing the highly-nonlinear state and measurement equations.

In this work, a new approach for on-board estimation of the mean elements from osculating element measurements is proposed. First, a semianalytical dynamical model that includes zonal/tesseral/sectorial harmonics and drag is formulated to capture the daily, long-periodic, and secular evolution of the mean orbital elements. Because there is a clear tradeoff between precision and complexity, the semianalytical model is truncated to include the control inputs, the long-periodic and secular terms up to $J_4/C_{33}/S_{33}$ and exponential drag. The mapping from mean to osculating elements, which is used as a measurement equation, is obtained by adding the short-periodic effects of drag and zonal/tesseral/sectorial harmonics to the mean elements. This unique formulation is then matched up with a square-root unscented Kalman filter (SR-UKF) [16] that serves as the mean elements estimator. The sigma point selection is performed based on the spherical simplex (SS) algorithm [17], which significantly reduces the number of propagated sigma points, thus allowing for improved computational efficiency and possible real-time implementation. A comprehensive performance evaluation for both controlled and uncontrolled orbits shows the potential advantages of the proposed filtering approach vis-à-vis Brouwer-type methods.

2 Preliminaries

In an inertial reference frame, the equations of motion for the perturbed Keplerian two-body problem are written as

$$\ddot{\mathrm{r}} + \frac{\mu}{r^3}\mathrm{r} = \mathrm{F} \tag{1}$$

where $\mathrm{r} \in \mathbb{R}^3 \backslash \{0\}$ is the position vector, $r = \|\mathrm{r}\|$ and F is the perturbation. The solution for the respective position and velocity vectors can be written as [18]

$$\mathrm{r} = \mathrm{f}_r\left[a(t), e(t), i(t), \Omega(t), \omega(t), M_0(t), t\right], \mathrm{v} = \mathrm{f}_v\left[a(t), e(t), i(t), \Omega(t), \omega(t), M_0(t), t\right] \tag{2}$$

where $\{a(t), e(t), i(t), \Omega(t), \omega(t), M_0(t)\}$ are the classical osculating orbital elements – semimajor axis, eccentricity, inclination, right ascension of the ascending node (RAAN), argument of perigee and mean anomaly at epoch, respectively. The variational equations for the classical elements are usually written in two forms. If $\mathrm{F} = \partial R/\partial \mathrm{r}$, for some perturbing potential R, then one obtains the Lagrange planetary equations (LPE) [18]

$$\frac{\mathrm{d}a}{\mathrm{d}t} = \frac{2}{\tilde{n}a}\frac{\partial R}{\partial M} \tag{3a}$$

$$\frac{\mathrm{d}e}{\mathrm{d}t} = \frac{1-e^2}{\tilde{n}a^2 e}\frac{\partial R}{\partial M} - \frac{\sqrt{1-e^2}}{\tilde{n}a^2 e}\frac{\partial R}{\partial \omega} \tag{3b}$$

$$\frac{\mathrm{d}i}{\mathrm{d}t} = \frac{\cot i}{\tilde{n}a^2\sqrt{1-e^2}}\frac{\partial R}{\partial \omega} - \frac{1}{\tilde{n}a^2\sqrt{1-e^2}\sin i}\frac{\partial R}{\partial \Omega} \tag{3c}$$

$$\frac{\mathrm{d}\Omega}{\mathrm{d}t} = \frac{1}{\tilde{n}a^2\sqrt{1-e^2}\sin i}\frac{\partial R}{\partial i} \tag{3d}$$

$$\frac{\mathrm{d}\omega}{\mathrm{d}t} = \frac{\sqrt{1-e^2}}{\tilde{n}a^2 e}\frac{\partial R}{\partial e} - \frac{\cot i}{\tilde{n}a^2\sqrt{1-e^2}}\frac{\partial R}{\partial i} \tag{3e}$$

$$\frac{\mathrm{d}M_0}{\mathrm{d}t} = -\frac{1-e^2}{\tilde{n}a^2 e}\frac{\partial R}{\partial e} - \frac{2}{\tilde{n}a}\frac{\partial R}{\partial a} \tag{3f}$$

where $\tilde{n} = \sqrt{\mu/a^3}$ is the mean motion.

A more general formulation of the variational equations, which allows for non-conservative specific forces, yields the Gauss variational equations (GVE). In the GVE, the perturbation is represented in **RSW**, i.e., $\Delta\mathrm{F} = F_R\hat{\mathrm{R}} + F_S\hat{\mathrm{S}} + F_W\hat{\mathrm{W}}$. The resulting equations are [18]:

$$\frac{\mathrm{d}a}{\mathrm{d}t} = \frac{2}{\tilde{n}\sqrt{1-e^2}}\left(e\sin f F_R + \frac{\tilde{p}}{r}F_S\right) \tag{4a}$$

$$\frac{\mathrm{d}e}{\mathrm{d}t} = \frac{\sqrt{1-e^2}}{\tilde{n}a}\left(\sin f F_R + \left(\cos f + \frac{e+\cos f}{1+e\cos f}\right)F_S\right) \tag{4b}$$

$$\frac{\mathrm{d}i}{\mathrm{d}t} = \frac{r\cos(\omega+f)}{\tilde{n}a^2\sqrt{1-e^2}}F_W \tag{4c}$$

$$\frac{\mathrm{d}\Omega}{\mathrm{d}t} = \frac{r\sin(\omega+f)}{\tilde{n}a^2\sqrt{1-e^2}\sin i}F_W \tag{4d}$$

$$\frac{\mathrm{d}\omega}{\mathrm{d}t} = \frac{\sqrt{1-e^2}}{\tilde{n}ae}\left(-\cos f F_R + \sin f\left(1+\frac{r}{\tilde{p}}\right)F_S\right) - \frac{r\cot i\sin(\omega+f)}{\sqrt{\mu\tilde{p}}}F_W \tag{4e}$$

$$\frac{\mathrm{d}M_0}{\mathrm{d}t} = \frac{1}{\tilde{n}a^2e}\left(\left(\tilde{p}\cos f - 2er\right)F_R - \left(\tilde{p}+r\right)\sin f F_S\right) \tag{4f}$$

where $\tilde{p} = a\left(1-e^2\right)$ is the semilatus rectum and f is the true anomaly.

With $\alpha \triangleq [a(t), e(t), i(t), \Omega(t), \omega(t), M_0(t)]$ as a state vector, and a mapping of the form $t \mapsto f(t,\alpha)$, the LPE (3) and GVE (4) can be written in a unified form as

$$\dot{\alpha} = \mathrm{g}(\alpha, t) \tag{5}$$

In many cases of interest, such as satellite orbit control, guidance and orbit propagation, the osculating elements are replaced by mean elements. A common definition of the mean elements relies on the averaging operator, which, for some given vector-valued function $\mathrm{s}(t)$, is defined by

$$\bar{\mathrm{s}} = \langle \mathrm{s}(t) \rangle \triangleq \frac{1}{T}\int_0^T \mathrm{s}\,\mathrm{d}t = \frac{1}{2\pi}\int_0^{2\pi} \mathrm{s}\frac{1}{\sqrt{1-e^2}}\left(\frac{r}{a}\right)^2 \mathrm{d}f = \frac{1}{2\pi}\int_0^{2\pi} \mathrm{s}\,\mathrm{d}M \tag{6}$$

where M is the mean anomaly. Thus, the mean elements are obtained by

$$\bar{\alpha} = \langle \alpha(t) \rangle \triangleq \frac{1}{T}\int_0^T \alpha(t)\,\mathrm{d}t \tag{7}$$

where T denotes the orbital period.

An analytical mean-elements calculation scheme was proposed by Kozai [6] and Brouwer [5], who used the averaging technique to isolate the short-periodic terms, α_{short}, so that

$$\bar{\alpha}(t) = \alpha(t) - \alpha_{short}(t) \tag{8}$$

Substituting Eq. (8) into Eq. (5) yields

$$\dot{\bar{\alpha}}(t) + \dot{\alpha}_{short}(t) = \mathbf{g} = \bar{\mathrm{g}} + \mathrm{g}_{short} \tag{9}$$

In this formulation, $\dot{\bar{\alpha}}(t)$ consists of secular and long-periodic terms, namely

$$\bar{\mathrm{g}} = \mathrm{g}_{sec} + \mathrm{g}_{long} \tag{10}$$

where

$$\mathrm{g}_{sec} = \mathrm{g}_{sec}\left(\bar{a}, \bar{e}, \bar{i}\right), \mathrm{g}_{long} = \mathrm{g}_{long}\left(\bar{a}, \bar{e}, \bar{i}, \bar{\Omega}, \bar{\omega}\right), \mathrm{g}_{short} = \mathrm{g}_{short}\left(\bar{a}, \bar{e}, \bar{i}, \bar{\Omega}, \bar{\omega}, \bar{M}\right) = \mathrm{g} - \bar{\mathrm{g}} \tag{11}$$

In the following discussion, this mean element calculation scheme will be coupled with a recursive filtering algorithm to yield accurate and computationally-tractable estimation of the mean elements.

3 Modeling the Orbital Dynamics

In this section, the semianalytical astrodynamical models used for the propagation of the mean elements will be discussed, including zonal, tesseral and sectorial harmonics, as well as drag.

3.1 The Zonal Part of the Geopotential

The perturbing gravitational potential including zonal harmonics only is given by [19]:

$$R_{zonal} = -\frac{\mu}{r}\sum_{n=2}^{\infty} J_n \left(\frac{r_e}{r}\right)^n P_n\left(\sin\varphi\right) \tag{12}$$

where $J_n, n = 2,3,\ldots$ are the zonal gravitational coefficients, φ is the latitude, $\sin\varphi = \sin i \sin u$, $u = \omega + f$ is the argument of latitude, r_e is Earth's mean equatorial radius and $P_n\left(x\right)$ denotes a Legendre polynomial of the first kind of order n, which is expressed as [20]

$$P_n\left(x\right) = \frac{1}{2^n n!}\frac{\mathrm{d}^n}{\mathrm{d}x^n}\left(x^2-1\right)^n \tag{13}$$

It is customary to average R_{zonal} prior to the substitution into the LPE (3). Applying the averaging operator (6) gives:

$$\bar{R}_{zonal} = \frac{1}{2\pi}\int_0^{2\pi} R_{zonal}\frac{1}{\sqrt{1-e^2}}\left(\frac{r}{a}\right)^2 \mathrm{d}f = R_{sec} + R_{long} \tag{14}$$

To evaluate the integral in Eq. (14), the zonal potential should be written as a function of the classical orbital elements. This procedure can be found in [19, 21].

3.2 Second-Order Effects

As pointed out by Brouwer [5], due to the nonlinear nature of the variational equations, the short-periodic terms contribute both secular and long-periodic inputs of $\mathscr{O}(J_2^2)$.

The resulting short-periodic averaged potential, after transforming into the classical orbital elements, is given by

$$\begin{aligned}\bar{R}_{short} = \frac{3J_2^2 r_e^4 \mu}{128\eta^7 a^5}\left[5\eta^2 - 4\eta - 5 - \cos^2 i\left(18\eta^2 - 24\eta - 10\right) + \right. \\ \left. \cos^4 i\left(5\eta^2 + 36\eta + 35\right) + e^2\left(30\cos^4 i - 32\cos^2 i + 2\right)\cos 2\omega\right]\end{aligned} \tag{15}$$

where $\eta = \sqrt{1-e^2}$.

3.3 The Tesseral-Sectorial Part of the Geopotential

The dominant tesseral and sectorial harmonics (degree 2 and order 2) have a period of approximately half day, which is much longer than the orbital period [19, 22]. Hence, tesseral and sectorial harmonics may have a significant effect on the long-periodic dynamics. It is thus imperative to include the tesseral and sectorial harmonics in the mean elements dynamical model. The perturbing gravitational potential of Tesseral and sectorial harmonics is given by [19]:

$$R_{Tesseral} = \frac{\mu}{r}\sum_{n=2}^{\infty}\sum_{m=1}^{n}\left(\frac{r_e}{r}\right)^n P_{nm}(\sin\varphi)\left[C_{nm}\cos m\lambda + S_{nm}\sin m\lambda\right] \tag{16}$$

where λ is the geographic longitude of the satellite measured eastward from the Greenwich meridian, C_{nm}, S_{nm} are harmonic coefficients and $P_{nm}(x)$ are the associated Legendre polynomials of degree n and order m, which are expressed as

$$P_{nm}(x) = \frac{1}{2^n n!}\left(1-x^2\right)^{\frac{m}{2}}\frac{\mathrm{d}^{n+m}}{\mathrm{d}x^{n+m}}\left(x^2-1\right)^n = \left(1-x^2\right)^{\frac{m}{2}}\frac{\mathrm{d}^m}{\mathrm{d}x^m}P_n(x) \tag{17}$$

The geopotential up to degree 3 and order 3 can be written down based on Eq. (16):

$$\begin{aligned}
R_{22} &= 3\cos^2\varphi\frac{\mu}{r}\left(\frac{r_e}{r}\right)^2\left(C_{22}\cos 2\lambda + S_{22}\sin 2\lambda\right) \\
R_{31} &= \frac{3}{2}\left(5\sin^2\varphi - 1\right)\frac{\mu}{r}\left(\frac{r_e}{r}\right)^3\left(C_{31}\cos\lambda + S_{31}\sin\lambda\right) \\
R_{32} &= 15\sin\varphi\cos^2\varphi\frac{\mu}{r}\left(\frac{r_e}{r}\right)^3\left(C_{32}\cos 2\lambda + S_{32}\sin 2\lambda\right) \\
R_{33} &= 15\cos^3\varphi\frac{\mu}{r}\left(\frac{r_e}{r}\right)^3\left(C_{33}\cos 3\lambda + S_{33}\sin 3\lambda\right)
\end{aligned} \tag{18}$$

Using the averaging method presented in Section 2, the long-periodic perturbing potentials of the tesseral and sectorial harmonics up to degree 3 and order 3 can be derived:

$$
\begin{aligned}
R_{long,22} &= \frac{3}{2}\sin^2 i\left(1-e^2\right)^{-\frac{3}{2}}\frac{\mu}{a}\left(\frac{r_e}{a}\right)^2\left(C_{22}\cos 2\Omega_s + S_{22}\sin 2\Omega_s\right)\\
R_{long,31} &= \frac{3}{2}e\left(1-e^2\right)^{-\frac{5}{2}}\frac{\mu}{a}\left(\frac{r_e}{a}\right)^3\left(\begin{array}{c} C_{31}\left(\cos\Omega_s\cos\omega\left(\frac{5}{4}\sin^2 i-1\right)+\sin\Omega_s\sin\omega\cos i\left(1-\frac{15}{4}\sin^2 i\right)\right)\\ +S_{31}\left(\cos\Omega_s\sin\omega\cos i\left(\frac{15}{4}\sin^2 i-1\right)+\sin\Omega_s\cos\omega\left(\frac{5}{4}\sin^2 i-1\right)\right)\end{array}\right)\\
R_{long,32} &= \frac{15}{4}e\left(1-e^2\right)^{-\frac{5}{2}}\sin^2 i\frac{\mu}{a}\left(\frac{r_e}{a}\right)^3\left(\begin{array}{c} C_{32}\left(\cos 2\Omega_s\sin\omega\left(3\sin^2 i-2\right)-2\sin 2\Omega_s\cos\omega\cos i\right)\\ +S_{32}\left(2\cos 2\Omega_s\cos\omega\cos i+\sin\Omega_s\sin\omega\left(3\sin^2 i-2\right)\right)\end{array}\right)\\
R_{long,33} &= \frac{45}{4}e\left(1-e^2\right)^{-\frac{5}{2}}\frac{\mu}{a}\left(\frac{r_e}{a}\right)^3\left(\begin{array}{c} C_{33}\left(2\cos 3\Omega_s\cos\omega\cos i+\sin 3\Omega_s\sin\omega\left(3\sin^2 i-2\right)\right)\\ +S_{33}\left(2\sin 3\Omega_s\cos\omega\cos i+\cos 3\Omega_s\sin\omega\left(2-3\sin^2 i\right)\right)\end{array}\right)
\end{aligned}
\tag{19}
$$

where $\Omega_s = \Omega - \theta$, and θ is the Greenwich sidereal angle.

3.4 Atmospheric Drag

The specific force due to atmospheric drag can be modeled as

$$
\mathrm{F}_{drag} = -\frac{1}{2}\frac{SC_D}{m}\rho\left(\mathbf{v}-\mathbf{v}_{atm}\right)\left\|\mathbf{v}-\mathbf{v}_{atm}\right\| \tag{20}
$$

where m is the satellite mass, S is the cross-sectional reference area, C_D is the drag coefficient defined with respect to the cross-sectional area, and ρ is the atmospheric density. The vector v_{atm} is the atmospheric velocity. If the atmosphere is assumed to be spherical and co-rotating with the Earth, then $\mathbf{v}_{atm} = \left[0\ 0\ \omega_e\right]^{\mathrm{T}} \times \mathrm{r}$.

The model used herein approximates the atmospheric density as [18]

$$
\rho = \rho_0 \exp\left(\frac{r_{p0}-r}{H}\right) \tag{21}
$$

where ρ_0 is the atmospheric density at the initial perigee radius, r_{p0}, and H is the density scale height of the atmosphere. The drag specific force vector $\mathbf{F}_{drag}$, written in terms of the osculating elements, can be expressed in the **NTW** frame as follows [23]:

$$
\begin{aligned}
F_T &= -\frac{1}{2}K_1\tilde{n}^2a^2\rho\frac{1+2e\cos f+e^2}{\left(1-e^2\right)}\\
F_N &= 0\\
F_W &= -\frac{1}{2}K_2\tilde{n}a\rho r\cos(\omega+f)\sin i\left(\frac{1+2e\cos f+e^2}{\left(1-e^2\right)}\right)^{1/2}
\end{aligned}
\tag{22}
$$

where $K_1 = (C_D S_1/m)\,Q$, $K_2 = (C_D S_2/m)\,\omega_e\sqrt{Q}$, and $Q = \left(1 - r_{p_0}\omega_e \cos i/v_{p_0}\right)^2$. The variables S_1 and S_2 are the respective cross-sectional areas perpendicular to the tangential and subnormal directions, and v_{p_0} is the velocity at the initial perigee. To use the GVE (4), the drag components are first transformed from **NTW** into **RSW** using the transformation

$$\begin{aligned} F_R &= \frac{e\sin f}{\sqrt{1+2e\cos f+e^2}}F_T + \frac{1+e\cos f}{\sqrt{1+2e\cos f+e^2}}F_N \\ F_S &= \frac{1+e\cos f}{\sqrt{1+2e\cos f+e^2}}F_T - \frac{e\sin f}{\sqrt{1+2e\cos f+e^2}}F_N \end{aligned} \tag{23}$$

Substituting Eqs. (22) and (23) into Eq. (4) yields:

$$\begin{aligned} \dot{a}_{drag} &= -\frac{K_1\tilde{n}a^2}{\left(1-e^2\right)^{3/2}}\rho\left(1+2e\cos f+e^2\right)^{3/2} \\ \dot{e}_{drag} &= -\frac{K_1\tilde{n}a}{\left(1-e^2\right)^{1/2}}\rho\left(\cos f+e\right)\left(1+2e\cos f+e^2\right)^{1/2} \\ \mathrm{d}i/\mathrm{d}t\,_{drag} &= -\frac{K_2 a}{4(1+e\cos f)^2}\rho\sin i\left(1+\cos\left(2(\omega+f)\right)\right)\left(1-e^2\right)\left(1+2e\cos f+e^2\right)^{1/2} \\ \dot{\Omega}_{drag} &= -\frac{K_2 a}{4(1+e\cos f)^2}\rho\sin\left(2(\omega+f)\right)\left(1-e^2\right)\left(1+2e\cos f+e^2\right)^{1/2} \\ \dot{\omega}_{drag} &= -\frac{K_1\tilde{n}a}{e\left(1-e^2\right)^{1/2}}\rho\sin f\left(1+2e\cos f+e^2\right)^{1/2} - \cos i\cdot\dot{\Omega}_{drag} \\ \dot{M}_{drag} &= -\frac{K_1\tilde{n}a}{e\left(1+e\cos f\right)}\rho\sin f\left(1+e\cos f+e^2\right)\left(1+2e\cos f+e^2\right)^{1/2} \end{aligned} \tag{24}$$

The atmospheric density can be expanded into a series dependant upon modified Bessel functions [24, 25], a procedure that results in the following variational equations for the secular terms,

$$\begin{aligned} \dot{a}_{drag,sec} &= -K_1\rho_0\tilde{n}a^2\left(1+e^2\left(\frac{3}{4}+\frac{a}{H}+\frac{a^2}{4H^2}\right)+\mathscr{O}\left(e^3\right)\right)\exp\left(\frac{r_{p_0}-a}{H}\right) \\ \dot{e}_{drag,sec} &= -K_1\rho_0\tilde{n}a\left(\frac{e}{2}+\frac{ae}{2H}+\mathscr{O}\left(e^3\right)\right)\exp\left(\frac{r_{p_0}-a}{H}\right) \\ \mathrm{d}i/\mathrm{d}t\,_{drag,sec} &= -\frac{1}{4}K_2\rho_0 a\sin i\left(1+e^2\left(\frac{3}{4}-\frac{a}{H}+\frac{a^2}{4H^2}\right)+\mathscr{O}\left(e^3\right)\right)\exp\left(\frac{r_{p_0}-a}{H}\right) \\ \dot{\Omega}_{drag,sec} &= 0 \\ \dot{\omega}_{drag,sec} &= 0 \\ \dot{M}_{drag,sec} &= \frac{3}{4}K_1\rho_0\tilde{n}^2 a\left(1+e^2\left(\frac{3}{4}+\frac{a}{H}+\frac{a^2}{4H^2}\right)+\mathscr{O}\left(e^3\right)\right)\exp\left(\frac{r_{p_0}-a}{H}\right)(t-t_0) \end{aligned} \tag{25}$$

while the long-periodic terms are given by:

$$\begin{aligned}
\dot{a}_{drag,long} &= 0 \\
\dot{e}_{drag,long} &= 0 \\
\mathrm{d}i/\mathrm{d}t\,_{drag,long} &= -\frac{1}{4}K_2\rho_0 a \sin i \left(\left(\frac{11}{8} - \frac{a}{H} + \frac{a^2}{8H^2}\right)e^2\cos 2\omega + \mathscr{O}\left(e^3\right)\right)\exp\left(\frac{r_{p_0}-a}{H}\right) \\
\dot{\Omega}_{drag,long} &= -\frac{1}{4}K_2\rho_0 a \left(\left(\frac{11}{8} - \frac{a}{H} + \frac{a^2}{8H}\right)e^2\sin 2\omega + \mathscr{O}\left(e^3\right)\right)\exp\left(\frac{r_{p_0}-a}{H}\right) \\
\dot{\omega}_{drag,long} &= -\cos i \cdot \dot{\Omega}_{drag,long} \\
\dot{M}_{drag,long} &= 0
\end{aligned} \tag{26}$$

Finally, the effect of the short-periodic terms can be obtained following the method of Kozai [6].

4 Mean Elements Estimator

The fully-assembled semianalytical model described in Section 3 may be written in the form

$$\begin{aligned}
\dot{\bar{\alpha}} = {} & \dot{\alpha}_{sec}\left(\bar{\alpha}\right) + \dot{\alpha}_{long}\left(\bar{\alpha}\right) + \dot{\alpha}_{sec,2}\left(\bar{\alpha}\right) + \dot{\alpha}_{long,2}\left(\bar{\alpha}\right) \\
& + \dot{\alpha}_{long,nm}\left(\bar{\alpha}\right) + \dot{\alpha}_{drag,sec}\left(\bar{\alpha}\right) + \dot{\alpha}_{drag,long}\left(\bar{\alpha}\right) + \mathrm{u}\left(\bar{\alpha}\right) + \mathrm{w}
\end{aligned} \tag{27}$$

where u denotes control inputs (either impulsive or continuous), whose effect is modeled using the GVE (4). The incorporation of the control forces using the GVE (4) involves an inherent approximation, since the GVE (4) are written in osculating elements. However, as previous studies have indicated, this approximation is adequate [3]. The vector w appearing in Eq. (27) is an additive process noise, which reflects modeling uncertainties. It is assumed that w is a white noise with power spectral density Q.

The satellite on-board sensors – e.g., a GPS receiver – provide measurements of the inertial position and velocity or unfiltered outputs for the osculating orbital elements by using the inverse of relations (2). Thus, in light of the discussion in Section 3, it is possible to write

$$\alpha_{osc} = \bar{\alpha} + \alpha_{short}\left(\bar{\alpha}\right) + \alpha_{drag,short}\left(\bar{\alpha}\right) + \alpha_{short,nm}\left(\bar{\alpha}\right) + \upsilon \tag{28}$$

where υ is the measurement noise, which is a discrete white noise process with the covariance matrix R.

It is readily seen that Eqs. (27) and (28) constitute nonlinear process and measurement equations, respectively, which adhere to the form

$$\dot{\mathrm{x}}(t_k) = \mathbf{f}(\mathrm{x}(t_k), t_k) + \mathbf{w}(t_k) \tag{29}$$

$$\mathbf{y}(t_k) = \mathbf{h}(\mathrm{x}(t_k)) + \upsilon(t_k) \tag{30}$$

where $\mathrm{x} \equiv \bar{\alpha} \in \mathbb{R}^n$ is the state vector, $\mathrm{y} \equiv \alpha_{osc} \in \mathbb{R}^n$ is the measurement vector, $\mathbf{f} : \mathbb{R}^n \times \mathbb{R}^+ \to \mathbb{R}^n$, and $\mathbf{h} : \mathbb{R}^n \to \mathbb{R}^n$. To obtain the estimated mean elements $\hat{\bar{\alpha}}$ from the osculating elements measurements, a nonlinear estimation algorithm should be used. In this work, the square-root form of the spherical simplex unscented Kalman filter (SR-UKF) is utilized.

As mentioned in the Introduction, the UKF is a sigma-point Kalman filter [26–28]. The square-root form of the UKF [16] provides improved numerical stability and keeps the covariance positive semidefinite. The spherical simplex sigma point selection method reduces the number of sigma points and decreases the computational time [17], and is hence more suitable for on-board real-time implementation. For completeness, the main steps necessary for the implementation of mean elements estimation based on the SR-UKF are elaborated herein.

4.1 Spherical Simplex Sigma-Point Selection

For an n-dimensional space, this sigma-point selection strategy provides $n+2$ sigma points, instead of the traditional $2n+1$ points. The point selection algorithm of the spherical simplex unscented transform for an n-dimensional system can be found in [17].

4.2 SR-UKF Algorithm

After the sigma points have been calculated, the SR-UKF can be applied as follows [16]:

(a) Calculate sigma points:

$$\chi_{k-1|i} = \hat{\mathrm{x}}_{k-1} + S_{\mathbf{x}_{k-1}} \mathrm{Z}_i, \qquad i = 0, \ldots, n+1 \tag{31}$$

where S_{x} denotes a Cholesky factor, initialized by taking $S_0 = \mathrm{chol}\left(E\left[\mathbf{x}_0 - \hat{\mathbf{x}}_0\right]\left[\mathbf{x}_0 - \hat{\mathbf{x}}_0\right]^{\mathrm{T}}\right)$, $\mathrm{chol}(\cdot)$ denotes the Cholesky factorization, and $\hat{\mathbf{x}}_0 = E[\mathbf{x}_0]$.

(b) Time update equations:

$$\dot{\chi}_{k-1|i} = \mathbf{f}(\mathbf{x}_{k-1}, t_{k-1}), \qquad i = 0, \ldots, n+1 \tag{32}$$

Discretization of the state equations will generally degrade the filter performance; Runge-Kutta integration is used instead for propagating the continuous

nonlinear state equations, avoiding discretization. Here $\chi_{k|i}$ is obtained. Now,

$$\hat{\mathbf{x}}_k^- = \sum_{i=0}^{n+1} w_i^m \chi_{k|i} \tag{33a}$$

$$S_{\mathbf{x}_k}^- = \mathrm{qr}\left(\left[\sqrt{w_1^c}\left(\chi_{k|1:n+1} - \hat{\mathbf{x}}_k^-\right), \sqrt{Q}\right]\right) \tag{33b}$$

$$S_{\mathbf{x}_k}^- = \mathrm{cholupdate}\left(S_{\mathbf{x}_k}^-, \chi_{k|0} - \hat{\mathbf{x}}_k^-, w_0^c\right) \tag{33c}$$

$$\chi_{k|i}^* = \hat{\mathbf{x}}_k^- + S_{\mathbf{x}_k}^- Z_i, \qquad i = 0, \ldots, n+1 \tag{33d}$$

$$\gamma_{k|i} = \mathbf{h}\left(\chi_{k|i}^*\right), \qquad i = 0, \ldots, n+1 \tag{33e}$$

$$\hat{\mathbf{y}}_k^- = \sum_{i=0}^{n+1} w_i^m \gamma_{k|i} \tag{33f}$$

where $\mathrm{qr}(\cdot)$ is a function that performs the QR decomposition, and $\mathrm{cholupdate}(\cdot)$ is a function that carries out the rank 1 Cholesky factor updating.

(c) Generate the Kalman gain and perform the measurement update:

$$S_{\mathbf{y}_k} = \mathrm{qr}\left(\left[\sqrt{w_1^c}\left(\gamma_{k|1:n+1} - \hat{\mathbf{y}}_k^-\right), \sqrt{R}\right]\right) \tag{34a}$$

$$S_{\mathbf{y}_k} = \mathrm{cholupdate}\left(S_{\mathbf{y}_k}, \gamma_{k|0} - \hat{\mathbf{y}}_k^-, w_0^c\right) \tag{34b}$$

$$P_{\mathbf{x}\mathbf{y}_k} = \sum_{i=0}^{n+1} w_i^c \left[\chi_{k|i} - \hat{\mathbf{x}}_k^-\right]\left[\gamma_{k|i} - \hat{\mathbf{y}}_k^-\right]^{\mathrm{T}} \tag{34c}$$

$$K_k = \left(P_{\mathbf{x}\mathbf{y}_k} / S_{\mathbf{y}_k}^{\mathrm{T}}\right) / S_{\mathbf{y}_k} \tag{34d}$$

$$\hat{\mathbf{x}}_k = \hat{\mathbf{x}}_k^- + K_k\left(\mathbf{y}_k - \hat{\mathbf{y}}_k^-\right) \tag{34e}$$

$$U = K_k S_{\mathbf{y}_k} \tag{34f}$$

$$S_{\mathbf{x}_k} = \mathrm{cholupdate}\left(S_{\mathbf{x}_k}^-, U, -1\right) \tag{34g}$$

where the operator A/B denotes the matrix division of B into A, i.e. a solution for x to the equation $AA^T\mathrm{x} = A^T B$ (see [29] for additional implementation details).

5 Results

The objective of this section is to evaluate the performance of the SS SR-UKF as a mean elements estimator subject to the semianalytical dynamical model. The mean elements estimation performance is evaluated using three test cases: Uncontrolled orbits (including a Monte-Carlo simulation), impulsive orbital corrections and continuous low-thrust orbital transfer. The "true" orbits are generated based on the High Precision Orbit Propagator in STK® , including a 21×21 gravity model (EGM96), drag according to the ISA-1976 model [30] and other perturbations, including solar radiation pressure, lunisolar third-body gravitational attraction and tides. For the

first example, a lifetime of one year is chosen so that the long-periodic terms, whose period is around five months, can manifest themselves in the orbital dynamics.

5.1 Initial Conditions and Parameter Values

The mission epoch is 1 Mar 2012 10:00:00.000 UTC, and it lasts until 28 Feb 2013 10:00:00.000 UTC. Table 1 gives the initial conditions in terms of osculating orbital elements.

The observation data are generated by contaminating the STK® -generated position and velocity vectors with GPS measurement errors. The one-sigma three-dimensional position and velocity errors are 5 m and 2 cm/s, respectively. The projection of the position and velocity measurement noise covariance onto osculating orbital elements space can be obtained by means of a Monte-Carlo simulation, yielding the results presented in Table 2, where the measurement noise covariance matrix R is given by

$$R = \mathrm{diag}\left[\mathrm{cov}_a, \mathrm{cov}_e, \mathrm{cov}_i, \mathrm{cov}_\Omega, \mathrm{cov}_\omega, \mathrm{cov}_M\right] \tag{35}$$

The time update was performed based on model (27), which included zonal harmonics up to J_4 and tesseral/sectorial terms up to C_{33}/S_{33}. Table 3 lists the numerical values of the geopotential coefficients and other parameters related to the astrodynamical models. The SS SR-UKF parameters are listed in Table 4.

Table 1: Initial osculating orbital elements values

Parameter	Numerical value
a	7000 km
e	0.01
i	55 deg
Ω	10 deg
ω	10 deg
M	10 deg

To obtain faster convergence, a judicious initialization of the estimated mean elements is required. To that end, the following initialization is used:

$$\hat{\bar{\alpha}}(t_0) = \alpha_{osc}(t_0) - \alpha_{short}\left(\alpha_{osc}(t_0)\right) - \alpha_{drag,short}\left(\alpha_{osc}(t_0)\right) \tag{36}$$

Equation (36) generates an approximation of the initial estimated values by replacing the mean elements with the (measured) osculating elements in the expressions for the short-periodic variations.

Table 2: Measurement noise covariance of the osculating orbital elements

Parameter	Numerical value
cov_a	$500.4\ \mathrm{m}^2$
cov_e	8.966×10^{-12}
cov_i	$1.886 \times 10^{-12}\ \mathrm{rad}^2$
cov_Ω	$9.020 \times 10^{-13}\ \mathrm{rad}^2$
cov_ω	$3.179 \times 10^{-8}\ \mathrm{rad}^2$
cov_M	$3.086 \times 10^{-8}\ \mathrm{rad}^2$

Table 3: Geopotential and drag model coefficients

Parameter	Numerical value
J_2	$1082.62668355 \times 10^{-6}$
J_3	$-2.53265648533 \times 10^{-6}$
J_4	$-1.61962159137 \times 10^{-6}$
C_{22}	$1.57446037456 \times 10^{-6}$
S_{22}	$-9.03803806639 \times 10^{-7}$
C_{31}	$2.19263852917 \times 10^{-6}$
S_{31}	$2.68424890297 \times 10^{-7}$
C_{32}	$3.08989206881 \times 10^{-7}$
S_{32}	$-2.11437612437 \times 10^{-7}$
C_{33}	$1.00548778064 \times 10^{-7}$
S_{33}	$1.97222559006 \times 10^{-7}$
ω_e	$7.2921158553 \times 10^{-5}\ \mathrm{rad/s}$
r_e	6378.137 km
μ	$3.98600436 \times 10^{14}\ \mathrm{m}^3/\mathrm{s}^2$
H	68.7 km
ρ_0	$2.34 \times 10^{-13}\ \mathrm{kg/m}^3$

Table 4: Filter parameters

Parameter	Numerical value
W_0	0.25
σ	1
β	0

5.2 Uncontrolled Orbits, Single Run

The simulation study starts by evaluating the ability of the filter to capture the long-periodic and secular mean element evolution for a one-year mission. The results are presented in Fig. 1, which compares the osculating and mean values of the semimajor axis (Fig. 1a), eccentricity (Fig. 1b), inclination (Fig. 1c), RAAN (Fig. 1d), and argument of perigee (Fig. 1e). It is evident that the filter captures the long-periodic evolution of the eccentricity and inclination and the slow secular evolution of the semimajor axis (due to atmospheric drag).

The next step is to evaluate the mean elements estimation errors. However, as opposed to standard filtering problems, in which the states of the process model are used as reference for comparing the estimated states, in the case at hand the semi-analytical model of the mean elements, given by Eq. (27), is truncated on purpose, and does not include effects such as lunisolar attraction, gravitational perturbations beyond order 4 and solar radiation pressure, to allow for computational efficiency. Thus, it makes little sense to use it as a reference for evaluating the estimation errors. Instead, a batch numerical averaging procedure is carried out to evaluate the "true" mean elements per definition (7). The batch averaging relies on the extended Simpson quadrature rule, given by [31]

$$\begin{aligned}\bar{\alpha} &= \frac{1}{T}\int_0^T \alpha(t)\,\mathrm{d}t = \frac{1}{N}\int_{t_0}^{t_{N-1}} \alpha(t)\,\mathrm{d}t \\ &= \frac{1}{N}\left(\frac{1}{3}\alpha(t_0)+\frac{4}{3}\alpha(t_1)+\frac{2}{3}\alpha(t_2)+\frac{4}{3}\alpha(t_3)+\right. \\ &\left.\cdots+\frac{2}{3}\alpha(t_{N-3})+\frac{4}{3}\alpha(t_{N-2})+\frac{1}{3}\alpha(t_{N-1})\right)+\mathscr{O}\left(\frac{1}{N^4}\right)\end{aligned} \tag{37}$$

where the alternation of $2/3$ and $4/3$ continues throughout the interior of Eq. (37). The vector of estimation errors is then defined as

$$\mathrm{e}_\alpha \triangleq \bar{\alpha} - \hat{\bar{\alpha}} \tag{38}$$

The estimation errors (38) are compared to a direct application of the Brouwer artificial satellite theory as formulated in Ref. [32]. The purpose of the comparison between the Brouwer and SS SR-UKF-based estimation of the mean elements is to inquire whether a direct application of the Brouwer theory may be used as a substitute for recursive filtering; as will be seen shortly, the answer to this question is strictly negative.

A comparison of estimation errors between the SS SR-UKF and the Brouwer theory is depicted in Fig. 2. In this figure, the estimation errors of the semimajor axis (Fig. 2a), eccentricity (Fig. 2b), inclination (Fig. 2c), RAAN (Fig. 2d) and argument of perigee (Fig. 2e) are shown for a 24-hour period to better illustrate the quantitative aspects of the differences between the Brouwer theory and the recursive filter. It is evident that the Brouwer-based errors are noisier than the filter-based estimation

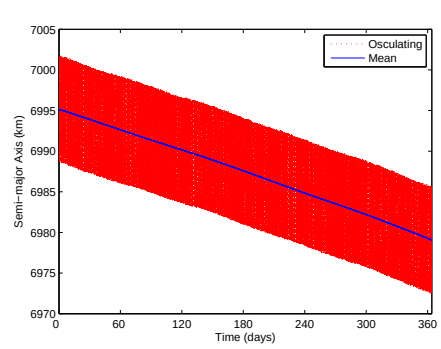

(a) Semimajor axis

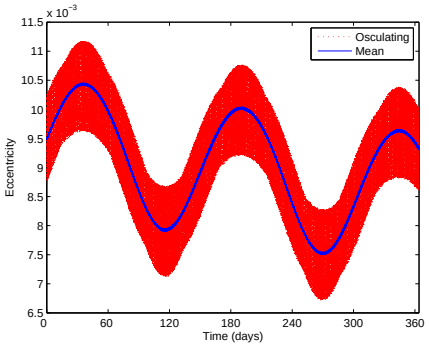

(b) Eccentricity

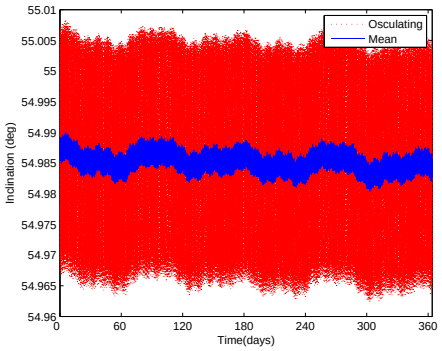

(c) Inclination

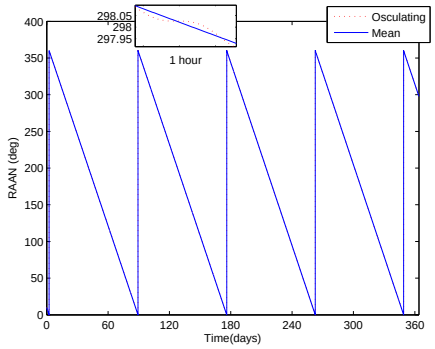

(d) RAAN

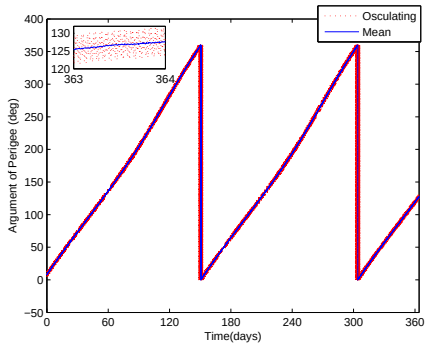

(e) Argument of perigee

Fig. 1: Sample single 1-year simulation run comparing the osculating and estimated mean orbital elements.

errors. In addition, the eccentricity estimation through Brouwer's theory is slightly biased, whereas in the filter-based estimation it is unbiased.

5.3 Uncontrolled Orbits, Monte-Carlo Runs

The observations in Section 5-5.2 can be substantiated using a long-term Monte-Carlo simulation. The numerical values of the standard deviations are summarized in Table 5. It is evident that the filter yields at least an order of magnitude better accuracy than the Brouwer theory. The difference is particularly dramatic in the estimation of the semimajor axis, wherein the filter provides a 1-σ accuracy of about 60 cm, compared to a Brouwer 1-σ value of about 22 m.

Table 5: Standard deviation values of the mean elements estimation errors for 100 Monte-Carlo Runs

σ	Filter	Brouwer
e_a	0.6118 m	22.42 m
e_e	3.972×10^{-7}	2.994×10^{-6}
e_i	9.380×10^{-6} deg	7.877×10^{-5} deg
e_Ω	6.665×10^{-6} deg	5.486×10^{-5} deg
e_ω	0.0013 deg	0.0103 deg

5.4 Continuous Thrust

The final test case involves continuous thrust. The magnitude of the thrust is $0.08N$, as used in the SAMSON mission [33] and the direction is determined by the unit vector $\left[\sqrt{3}/3\ ,\sqrt{3}/3\ ,\sqrt{3}/3\ \right]$ in the **NTW** frame, indicating that all three maneuver channels are active. A thrusting arc of 3 hours is used. The results for a 12-hour integration are shown in Fig. 3. Although the acceleration caused by the continuous thrusting induces both secular and periodic variations in the mean elements, the filter is capable of providing unbiased estimation of the mean elements, including the semimajor axis (Fig. 3a), eccentricity (Fig. 3b), inclination (Fig. 3c), RAAN (Fig. 3d) and argument of perigee (Fig. 3e).

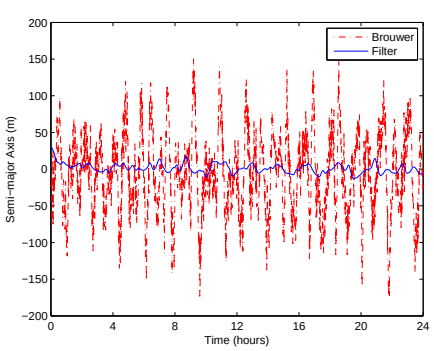

(a) Semimajor axis

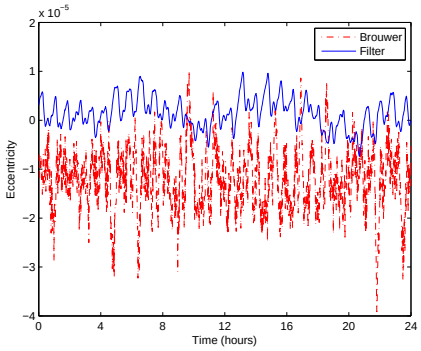

(b) Eccentricity

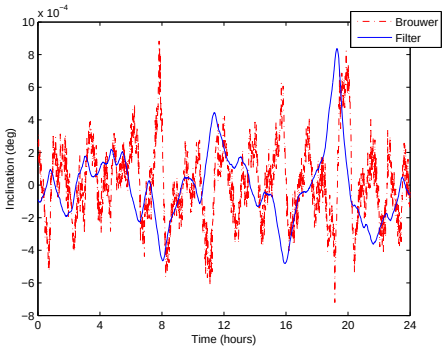

(c) Inclination

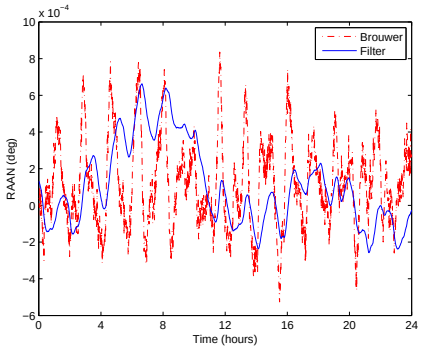

(d) RAAN

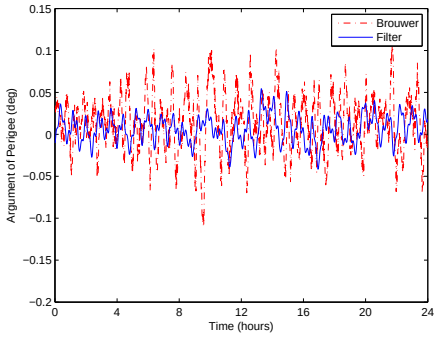

(e) Argument of perigee

Fig. 2: Sample simulation run comparing the mean element estimation errors as obtained from the Brouwer theory and the SS SR-UKF filter.

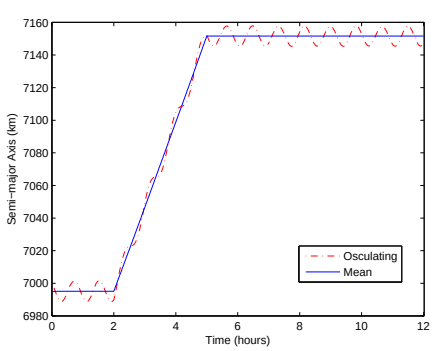

(a) Semimajor axis

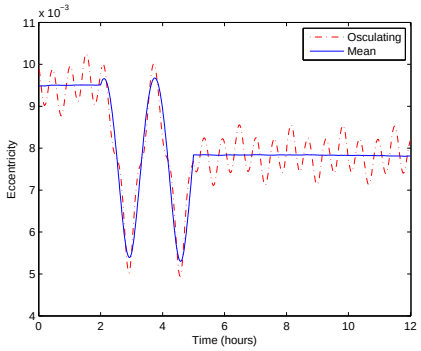

(b) Eccentricity

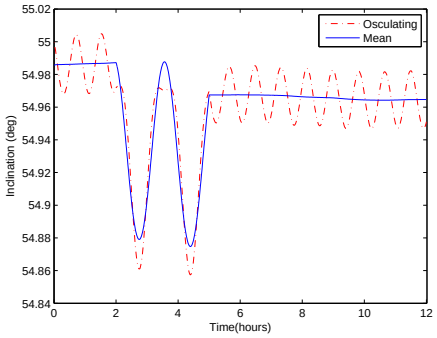

(c) Inclination

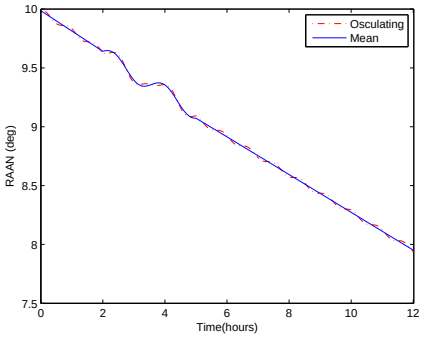

(d) RAAN

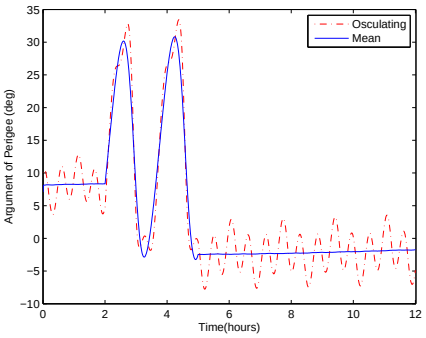

(e) Argument of perigee

Fig. 3: Estimated mean elements under continuous constant-magnitude low thrust. The SS SR-UKF provides unbiased estimation of the mean elements for a 3-hour thrusting arc.

6 Conclusions

Using the spherical simplex square-root unscented Kalman filter for estimating the mean orbital elements has clear advantages over the Brouwer artificial satellite theory: It can adequately respond to thrust, and it is much less sensitive to measurement noise. In the examined scenarios, the filter provided a sub-meter 1-σ estimation accuracy of the mean semimajor axis, which is almost two orders of magnitude better than the Brouwer-based estimation. The filter was designed from an astrodynamical standpoint – the equations were formulated in a True of Date reference frame, thus taking into account the precession and nutation of the Earth; tesseral and sectorial harmonics were not neglected, thus yielding improved estimation of the inclination and eccentricity variations; and the short-periodic effects were used to transform from mean to osculating elements.

Acknowledgments

This work was supported by the European Research Council Starting Independent Researcher Grant # 278231: Flight Algorithms for Disaggregated Space Architectures (FADER).

References

1. Chobotov, V., *Orbital Mechanics*, Vol. 1, AIAA, 2002, Chapter 14, pp. 335-409.
2. Gao, Y., "Low-thrust Nonlinear Guidance by Tracking Mean Orbital Elements," *Journal of Guidance, Control, and Dynamics*, Vol. 31, No. 4, 2008, pp. 1103–1110.
3. Schaub, H. and Alfriend, K. T., "Impulse Feedback Control to Establish Specific Mean Orbit Elements of Spacecraft Formations," *Journal of Guidance, Control and Dynamics*, Vol. 24, No. 4, 2001, pp. 739–745.
4. Salama, O., "Autonomous Orbit Maintenance Law for LEO Sun Synchronous, Earth Repeating Satellites with Electric Propulsion System," *AIAA/AAS Astrodynamics Specialist Conference and Exhibit*, Honolulu, Hawaii, USA, August 2008, AIAA Paper 2008-7197.
5. Brouwer, D., "Solution of the Problem of Artificial Satellite Theory without Drag," *The Astronomical Journal*, Vol. 64, 1959, pp. 378–396.
6. Kozai, Y., "The Motion of A Close Earth Satellite," *The Astronomical Journal*, Vol. 64, 1959, pp. 367–377.
7. Brouwer, D. and Hori, G. I., "Theoretical Evaluation of Atmospheric Drag Effects in the Motion of an Artificial Satellite," *The Astronomical Journal*, Vol. 66, 1961, pp. 193–225.
8. Liu, J. J. F. and Alford, R. L., "Semianalytic Theory for a Close-Earth Artificial Satellite," *Journal of Guidance, Control, and Dynamics*, Vol. 3, No. 4, 1980, pp. 304–311.
9. Liu, J. J. F., "Advances in Orbit Theory for an Artificial Satellite with Drag," *Journal of the Astronautical Sciences*, Vol. 31, No. 2, 1983, pp. 165–188.
10. Liu, J. J. F. and Alford, R. L., "A Semi-analytic Theory for the Motion of a Close-earth Artificial Satellite with Drag," *AIAA, Aerospace Sciences Meeting*, New Orleans, LA, USA, January 1979, AIAA Paper 79-0123.

11. Lane, M. H., "The Development of an Artificial Satellite Theory Using a Power-law Atmospheric Density Representation," *AIAA Second Aerospace Sciences Meeting, New York, NY, USA*, January 1965, AIAA Paper 65-35.
12. Lane, M. H., Fitzpatrick, P. M., and Murphy, J. J., "On the Representation of Air Density in Satellite Deceleration Equations by Power Functions with Integral Exponents," Tech. rep., DTIC Document, 1962, Report No. APGC-TDR-62-15.
13. Hoots, F. R., "Theory of the Motion of an Artificial Earth Satellite," *Celestial Mechanics and Dynamical Astronomy*, Vol. 23, No. 4, 1981, pp. 307–363.
14. Lin, L. and De-zi, Z., "Combined Perturbation on Near-earth Satellite Orbits," *Chinese Astronomy and Astrophysics*, Vol. 5, No. 4, 1981, pp. 422–433.
15. Bezdek, A. and Vokrouhlickı, D., "Semianalytic Theory of Motion for Close-earth Spherical Satellites Including Drag and Gravitational Perturbations," *Planetary and Space Science*, Vol. 52, No. 14, 2004, pp. 1233–1249.
16. Van Der Merwe, R. and Wan, E., "The Square-root Unscented Kalman Filter for State and Parameter-estimation," *IEEE International Conference on Acoustics, Speech, and Signal Processing*, Vol. 6, IEEE, 2001, pp. 3461–3464.
17. Julier, S., "The Spherical Simplex Unscented Transformation," *Proceedings of theAmerican Control Conference*, Vol. 3, IEEE, 2003, pp. 2430–2434.
18. Battin, R., *An Introduction to the Mathematics and Methods of Astrodynamics*, AIAA, 1999, Chapter 10, pp. 471-514.
19. Vallado, D. and McClain, W., *Fundamentals of Astrodynamics and Applications*, Vol. 21, Springer, 2007, Chapter 9, pp. 605-693.
20. Lambeck, K., *Geophysical Geodesy*, Clarendon Press, Oxford, UK, 1988, Chapter 5, pp. 171-215.
21. Liu, L., Hu, S. J., and Wang, X., *An Introduction to Astrodynamics*, Nanjing University Press, 2006, Chapter 4, pp. 90-114.
22. Liu, L., *Orbit Theory of Spacecraft*, National Defence Industry Press, 2000, Chapter 4, pp. 114-148.
23. Liu, L. and Zhao, D., "Combined Perturbation on Near-earth Satellite Orbits," *Chinese Astronomy and Astrophysics*, Vol. 5, 1981, pp. 422–433.
24. Brouwer, D. and Clemence, G. M., "Methods of Celestial Mechanics," *Academic Press, NY*, Vol. 1, 1961, pp. 45–122.
25. Breiter, S. and Metris, G., "Keplerian Expansions in Terms of Henrard's Practical Variables," *Celestial Mechanics and Dynamical Astronomy*, Vol. 58, No. 3, 1994, pp. 237–244.
26. Julier, S., Uhlmann, J., and Durrant-Whyte, H., "A New Approach for Filtering Nonlinear Systems," *Proceedings of the American Control Conference*, Vol. 3, IEEE, 1995, pp. 1628–1632.
27. Julier, S., Uhlmann, J., and Durrant-Whyte, H. F., "A New Method for the Nonlinear Transformation of Means and Covariances in Filters and Estimators," *IEEE Transactions on Automatic Control*, Vol. 45, No. 3, 2000, pp. 477–482.
28. Haykin, S. et al., *Kalman Filtering and Neural Networks*, Wiley Online Library, 2001, Chapter 7, pp. 221-269.
29. Alfriend, K. T., Gurfil, P., Vadali, S. R., How, J. P., and Breger, L., *Spacecraft Formation Flying: Dynamics, Control, and Navigation*, Butterworth-Heinemann, 2010, Chapter 3, pp. 39-52.
30. Noaa, N. and Usaf, U., "Standard Atmosphere, 1976," *US Government Printing Office, Washington, DC*, 1976.
31. Press, W., Teukolsky, S., Vetterling, W., and Flannery, B., *Numerical Recipes 3rd Edition: The Art of Scientific Computing*, Cambridge University Press, 2007, Chapter 4, pp. 160.
32. Schaub, H. and Junkins, J. L., *Analytical Mechanics of Space Systems*, Vol. 1, AIAA, 2003, pp. 573-576.
33. Gurfil, P., Herscovitz, J., and Pariente, M., "The SAMSON Project - Cluster Flight and Geolocation with Three Autonomous Nano-satellites," *26th AIAA/USU Conference on Small Satellites*, Salt Lake City, UT, USA, August 2012, Paper SSC12-VII-2.